ARMY RESEARCH LABORATORY

Development of a Miniature Snapshot Multispectral Imager

by Neelam Gupta, Philip R. Ashe, and Songsheng Tan

ARL-TR-5320 **September 2010**

NOTICES

Disclaimers

The findings in this report are not to be construed as an official Department of the Army position unless so designated by other authorized documents.

Citation of manufacturer's or trade names does not constitute an official endorsement or approval of the use thereof.

Destroy this report when it is no longer needed. Do not return it to the originator.

Army Research Laboratory
Adelphi, MD 20783-1197

ARL-TR-5320 **September 2010**

Development of a Miniature Snapshot Multispectral Imager

Neelam Gupta
Sensors and Electron Devices Directorate, ARL

Philip R. Ashe[*] and Songsheng Tan
Infotonics Technology Center, 5450 Campus Drive
Canandaigua, NY 14424

[*]Presently at SpectralSight, Inc.
2 Mae Meadow, Rochester, NY 14624

REPORT DOCUMENTATION PAGE

Form Approved
OMB No. 0704-0188

1. REPORT DATE *(DD-MM-YYYY)*	2. REPORT TYPE	3. DATES COVERED (From - To)
September 2010	Final	March 2008–December 2009

4. TITLE AND SUBTITLE
Development of a Miniature Snapshot Multispectral Imager

5a. CONTRACT NUMBER
W911NF-07-2-0004

5b. GRANT NUMBER

5c. PROGRAM ELEMENT NUMBER

6. AUTHOR(S)
Neelam Gupta[a], Philip R. Ashe[b*], and Songsheng Tan[b]

5d. PROJECT NUMBER

5e. TASK NUMBER

5f. WORK UNIT NUMBER

7. PERFORMING ORGANIZATION NAME(S) AND ADDRESS(ES)
U.S. Army Research Laboratory
ATTN: RDRL-SEE-E
2800 Powder Mill Road
Adelphi, MD 20783-1197

8. PERFORMING ORGANIZATION REPORT NUMBER
ARL-TR-5320

9. SPONSORING/MONITORING AGENCY NAME(S) AND ADDRESS(ES)

10. SPONSOR/MONITOR'S ACRONYM(S)

11. SPONSOR/MONITOR'S REPORT NUMBER(S)

12. DISTRIBUTION/AVAILABILITY STATEMENT
Approved for public release; distribution unlimited.

13. SUPPLEMENTARY NOTES
[a]U.S. Army Research Laboratory, 2800 Powder Mill Road, Adelphi, MD, USA 20783-1197
[b]Infotonics Technology Center, 5450 Campus Drive, Canandaigua, NY, USA 14424
[*]Presently at SpectralSight, Inc., 2 Mae Meadow, Rochester, NY, USA 14624

14. ABSTRACT

We present a miniature snapshot multispectral imager that operates in the short wavelength infrared (SWIR) region and has a number of applications. The system is low weight and portable with a miniature platform, and requires low power. The imager uses a 4×4 Fabry-Perot filter array operating from 1487 to 1769 nm with a spectral bandpass ~10 nm. The design of the filters is based on using a microelectromechanical system (MEMS) shadow mask technique to fabricate a Fabry-Perot etalon with multilayer dielectric mirrors. The filter array subsystem is installed in a commercial handheld indium gallium arsenide (InGaAs) camera, replacing the imaging lens with a custom designed 4×4 microlens array with telecentric imaging performance in each of the 16 sub imaging channels. We imaged several indoor and outdoor scenes. The microlens optics and filter design is quite flexible and can be tailored for any wavelength region from ultraviolet (UV) to longwave infrared (LWIR) and the spectral bandpass can also be customized to meet requirements. In this report, we discuss the design and characterization of the filter array, microlens optical package, and imager and present the imaging results. A main motivation behind development of such a compact imager is to be able to detect chemicals used in improvised explosive devices (IEDs).

15. SUBJECT TERMS
Fabry-Perot filter, multispectral, SWIR, microlens optics, IED detection

16. SECURITY CLASSIFICATION OF:			17. LIMITATION OF ABSTRACT	18. NUMBER OF PAGES	19a. NAME OF RESPONSIBLE PERSON
a. REPORT	b. ABSTRACT	c. THIS PAGE			Neelam Gupta
Unclassified	Unclassified	Unclassified	UU	34	19b. TELEPHONE NUMBER (*Include area code*) (301) 394-2451

Contents

List of Figures

List of Tables

INTENTIONALLY LEFT BLANK.

1. Introduction

Development of compact multispectral imaging sensors with no moving parts is required for many defense, medical, environmental monitoring, and variety of other applications. A multispectral imager uses an optical device that can separate the colors to obtain the spectral content in the scene. Such an optical device could be a grating or prism, a filter wheel, a diffractive optic lens, a Fabry-Perot (F-P) etalon, or a tunable filter. All of these optical devices are used with a focal plane array (FPA) and suitable optics for a given spectral region. All such imagers collect images in a time sequential manner. Recently, some multispectral imagers have been developed that collect images of the scene at all the spectral bands simultaneously (*1–5*). We describe one such imager that has been developed using microelectromechanical system (MEMS) technology to fabricate a filter bank covering a spectral region with each filter operating at a specific peak wavelength with a design spectral width. Such a filter array is then combined with a microlens assembly based on telecentric design to image the same scene at each spectral band without much overlap with neighboring bands using a honeycomb baffle design at a subsection of the FPA. Recently, a snapshot miniature multispectral imaging system operating in the shortwave infrared (SWIR) region has been developed by the U.S. Army Research Laboratory (ARL) working with the Infotonics Technology Center (ITC), Canandaigua, NY. One of the main motivations behind development of such a compact imager is to be able to detect chemicals used in improvised explosive devices (IEDs).

The two main components used in the design of such a snapshot multispectral imager are the multichannel F-P filter array and the microlens assembly. The filter array uses 16 F-P etalons, each tuned to a different peak wavelength. The filter bank consists of a 4×4 two-dimensional (2-D) array of fixed wavelength filters each with a narrow bandpass. The filter design was arrived at after a lot of research effort had been devoted to finding the proper materials, mirror design, and thin-film deposition techniques. Instead of using two high reflectivity metal mirrors with a cavity in between to fabricate each of the 16 F-P filters, a multilayer dielectric stack mirror design was chosen to obtain optimal filter performance. Each of the mirrors on either side of the cavity in the F-P etalon was fabricated using 11 alternating layers of two different dielectric materials: titanium dioxide (TiO_2) and silicon dioxide (SiO_2) with different refractive index values. In the mirror design, the layer thickness for each material was chosen equal to one quarter of the selected center wavelength of the filter to obtain the desired spectral full width at half maximum (FWHM) with high filter finesse. A SIO_2 cavity between the two dielectric mirrors was chosen with a corresponding thickness for each of the peak wavelengths. Each of the 16 F-P filters had the same top and bottom multilayer dielectric mirror but the cavity thickness for each filter was different, equal to around one half of the corresponding center wavelength of the filter. The F-P filters were fabricated by deposition of evaporated thin material films. Different cavity layer thicknesses for the 16 spectral filters were achieved by using only four

shadow masks for deposition of the evaporated SiO_2 films. The other main component that is required to obtain simultaneous multispectral images of a scene is a microlens assembly that can image the scene into 16 different spectral channels, coming through each filter on a subsection of the FPA of the SWIR camera independently, i.e., the out-of band leakage from the surrounding filters has to be made as small as possible. This was achieved by using two arrays of 4×4 microlenses with field stops and baffles. Commercial-off-the-shelf lenses were used with some machining to match the size of the individual filter. The f-number of microlenses, baffle thickness, and field stop distances were chosen after careful radiometric considerations to optimize the light transmission to the FPA. The filter bank operates from 1487 to 1769 nm with a spectral bandpass ~10 nm. The design of the filter array can be customized for any spectral region from the ultraviolet (UV) to the longwave infrared (LWIR). Also, filter and custom optics sizes can be matched to optimize performance using a variety of cameras with different size focal planes. The fabricated filter was installed in front of a commercial camera with an indium gallium arsenide (InGaAs) FPA and the camera imaging lens was replaced by the microlens assembly. The microlens assembly was carefully tested with the commercial camera for its 4×4 independent image formation capability. A number of filter arrays were fabricated and carefully characterized for their spectral characteristics. The snapshot multispectral imager with 16 independent channels was carefully calibrated to evaluate its imaging performance. A number of indoor and outdoor scenes were imaged and the images were analyzed. In this report, we discuss the snapshot imager concept (section 2); the micro optic assembly design and testing (section 3); the filter design, fabrication and characterization (section 4); the snapshot imager and its imaging performance (section 5), and finally the results and conclusions (sections 6 and 7, respectively).

2. Snapshot Multispectral Imager Concept

The snapshot imager is designed using a commercial camera without its imaging lens, a 2-D filter bank that contains a number of filters each transmitting at a different peak wavelength in front of the FPA, and a microlens assembly in front of the filter array to ensure a telecentric light path through the F-P filters and to image the scene on the corresponding subsections of FPA. In figure 1, we show a computer aided design of such an imaging system. A cut-off filter is shown in front of the camera to control the spectral spread of the incident light such that only the first order images from the F-P filters will be formed on the FPA. The micro optic package was designed to image the light transmitting through each filter independently on a subsection of the FPA without any leakage from the surrounding filters. This requires using a light stop array and baffles with the microlens array to ensure telecentric light paths to meet the F-P etalon requirements. The main design consideration is to form images on the FPA using only close to normal incident light.

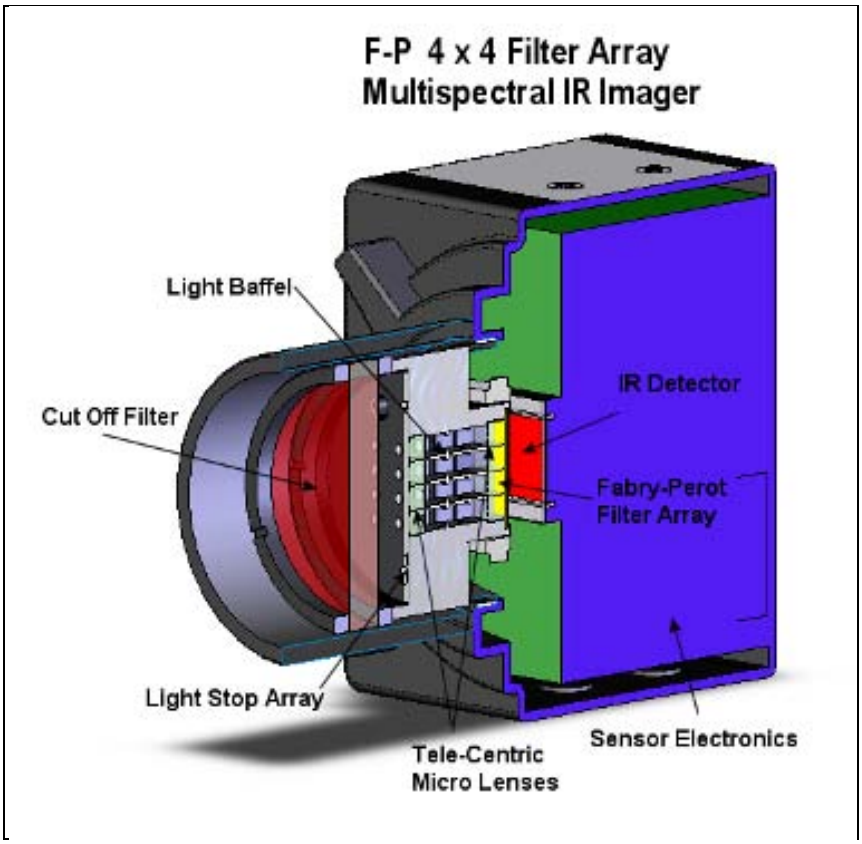

Figure 1. An illustration of snapshot multispectral imager using a commercial camera. A 4×4 filter array is installed in front of the FPA and in front of the filter array a micro optic assembly with telecentric microlenses, baffles, and light stop array are placed.

To find the required IR camera, the following parameters were considered: range of operation, camera resolution, pixel size, FPA size, temperature setting required for operation, ease of operation, availability, and cost. The camera that best fit these requirements was a Goodrich Sensors Unlimited model SU3201.7RT camera with 320×240 pixels with a 12.8×9.6 mm size InGaAs FPA with a 40-μm pixel pitch and a spectral range of 0.9–1.7 μm at room temperature operation (*6*). The size of the individual filters in the array and the custom optical package with microlenses was designed to work with this camera. The other camera that was considered was a Goodrich model SU640KTSX, which has an InGaAs FPA with 640×512 pixels and a 25-μm pixel pitch. In addition, Goodrich is developing a 1920×1080 pixel IR camera in the near future. As stated earlier, the filter and microlens package can be redesigned to fit other FPAs and lens working distances.

3. Design of Micro Optic Assembly

The optical design goal was to create a lens system that would output a matrix of identical images of the captured scene simultaneously and project these parallel images through the image stop, microlenses, light baffle, another set of micro lenses, and filter array and onto the sensor as described in patent application U.S. 11/995362 (*7*). The design goals were to maximize the camera output performance, maintain the light ray angular specification of an F-P, and meet the operating requirements of the imager.

The optical design* illustrated in figure 2 has been customized to match the focal plane of an InGaAs camera model SU3201.7RT with a 320×240 FPA format with a 40-μm pixel pitch. The design is essentially a compact array of 16 (4×4) sub-imaging optical systems. Each sub-imager consists of an optical stop and two lenses with the front lens spaced from the rear so that the imaging is telecentric on the image side, as shown in figure 2.

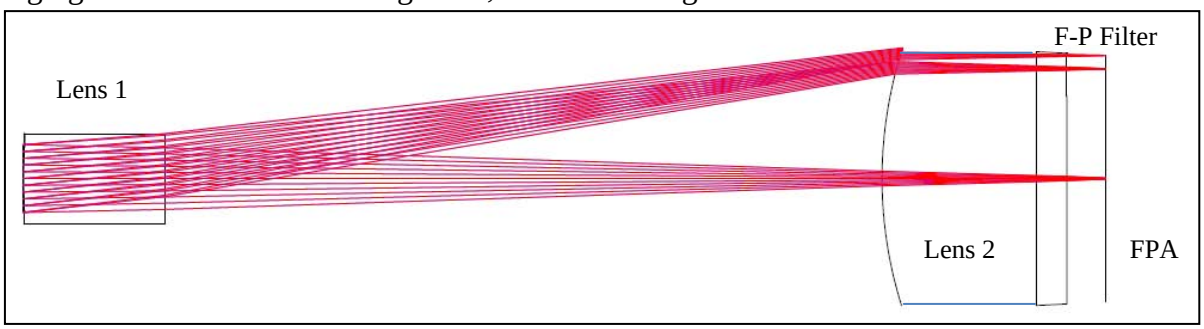

Figure 2. Single imaging channel of multiple channel imager composed of (as viewed from left to right)—front lens, rear lens, narrow-band F-P filter, and FPA. Not shown in the figure is the optical stop in front of lens 1.

The telecentricity in each channel is achieved by placing the front lens one focal length (rear lens focal length, F2) away from the rear lens. Telecentricity accomplishes the objective of minimizing the angles through the narrowband F-P filter. A free parameter is the focal length F1 assigned to the front lens. This parameter determines the field coverage and the F# of each channel, as shown in figure 3. The distance, h, to the FPA, as shown in figure 3, is 2 mm. The x- and y-pitch to meet the desired cell size constrains much of the design. In the present design, the top and bottom lenses were mechanically modified to fit the optical assembly. In future, when significant volumes are desired, monolithic lens arrays may be preferable. One system tradeoff is with the system F# (Fno_det) and the roll-off in the field due to vignetting of the ray bundle. Filling the front lens aperture diameter (2y1) produces the lowest F#, but roll-off begins immediately. It can be shown that the sensitivity of InGaAs FPA allows F#'s between 10–15 with good signal-to-noise ratio from sunlit scenes. This, in turn, allows much of the sub-image

*Optical design and simulations by Chris Brophy, OES, Rochester, NY.

area to be unvignetted. An array of 1-mm-diameter aperture stops is placed in front of the front lenses. The out-of-band image leakage is very small when compared to the light rays captured at the sub-section of FPA for each channel. Edge roll-off and sub-image size with a light baffle wall thickness of 0.3 mm gives an image size of 48×70 pixels. Simulation results for this are shown in figure 4.

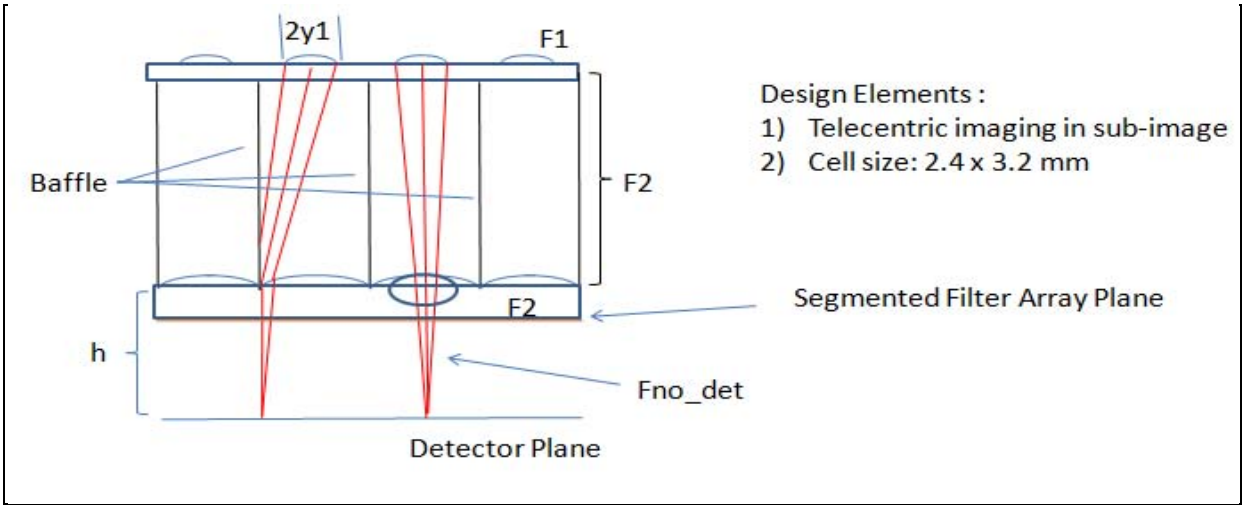

Figure 3. Design of micro optic assembly. Off-the-shelf plano-convex lenses were selected and reshaped to fit the assembly. Plano-convex lenses focus a collimated beam to the back focus and collimate light from a point source. Two different plano-convex lenses were chosen one with a focal length of 15 mm and a second with a focal length of 10.2 mm with anti-reflection coating for the operation in the desired spectral region. The F# of the micro optic for each channel is 10.2.

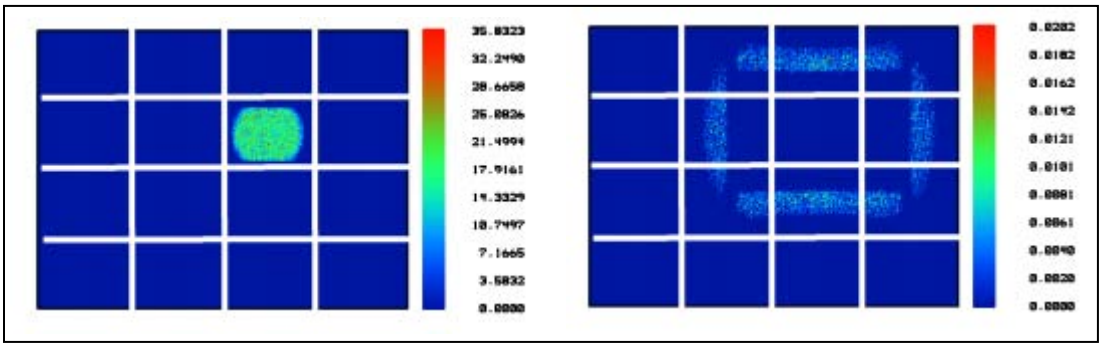

Figure 4. Simulation showing in-band and out-of-band images using the optical assembly and F-P filter array. The out-of-band image leakage is very small when compared to the light rays captured at the detector edge.

3.1 Optical Performance

3.1.1 Optical Parameters

- Working F# (channel): 10.2
- Strehl Ratio (worst-case field, ($1.4 < \lambda < 1.8$ μm)): 97%

Full Field of View: 10.2° (along 2.4 mm length) × 13.6° (along 3.2 mm length)

3.1.2 Tolerance Analysis

- Worst-case sensitivity to relative decentering of the two lenses (field tilt): Strehl (±0.1 mm decenter) = > 91%; (±0.052 mm decenter) = > 95%

For either case, there is a negligible reduction in image quality due to the large (40-μm) pixel pitch. In fact, a sensor with pixels half this size would still experience negligible image degradation.

3.1.3 1st-order Radiometric Analysis

Irradiance, I_r, the incident radiant power per unit area on the FPA is given by the following expression (*8*):

$$I_r = \Omega L T, \tag{1}$$

where L is the source radiance, Ω is the solid angle of collection, and T is the overall optical transmission of the imaging system, given by

$$T = T_{op} T_{FP}, \tag{2}$$

where T_{op} is the transmission of the optics including the cutoff filter before the microlenses and T_{FP} is the transmission of the each FP etalon. For the InGaAs FPA, sensor noise equivalent irradiance, *NEI* = 0.13 nW/cm^2 (near 1.55 μm, with quantum efficiency, QE = 80%) (*6*). We will denote NEI by I_n. Since the solid angle, Ω, for optics for each channel is given by $\pi/(4F\#^2)$, we can obtain an expression for L by using the fact that minimum irradiance on FPA that gives rise to *NEI*:

$$NEI \equiv I_r = \frac{\pi L T}{4F\#^2}. \tag{3}$$

Using equations 2 and 3, we can write

$$L = \frac{4F\#^2 I_n}{\pi T_{op} T_{FP}}. \tag{4}$$

Based on the imager design, the values of these parameters are I_n = 0.13 nW/cm^2; F# = 10.2; T_{FP} = 0.8, and T_{FP} = 0.5. Substituting these values in equation 4, we obtain L = 43 nW/cm^2-ster. Since the noise-equivalent radiance, *NEL*, is defined as the dimmest scene radiance that gives rise to the camera *NEI*, from the above calculations, *NEL* ~ 43 nW cm^{-2}-ster^{-1}. This is a reasonable value for a scene illuminated by the sun. The incident radiance around 1.55 μm on the camera is over 2000 times greater than *NEL*, which means that there should be adequate S/N for the camera with the chosen design parameters.

3.2 Microlens Assembly Prototypes

Figure 5 shows the microlens assembly viewed from top and bottom.

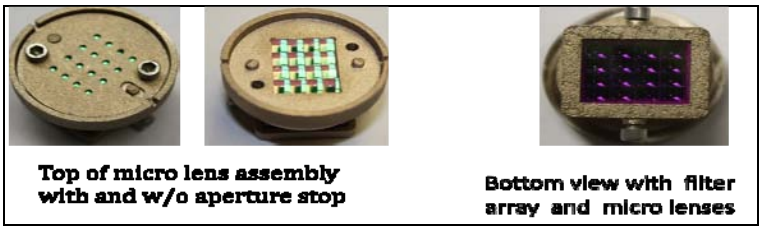

Figure 5. Different views of microlens assembly.

3.3 Characterization of Microlens Assembly

The microlens assembly was installed in front of the IR camera and some images were acquired to understand the image formation and see the effect of the baffles, as shown in figure 6. An object was illuminated with a monochromatic light using a 1560-nm filter in front of an incandescent light source and images were captured with the camera.

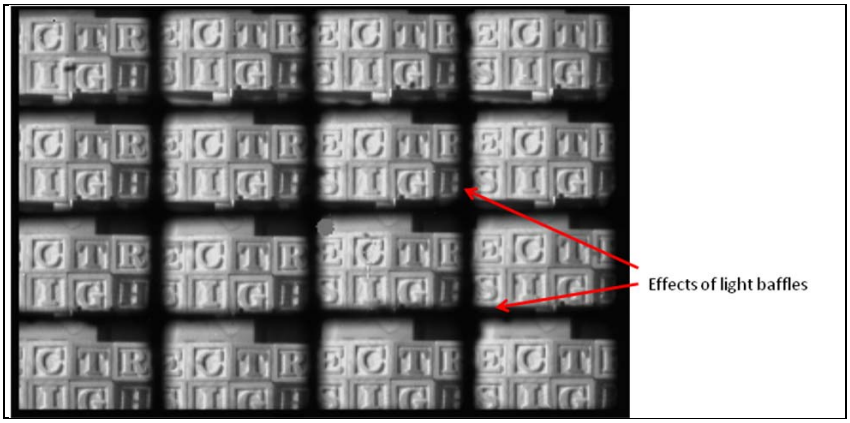

Figure 6. Monochromatic images captured from 16 channels of the microlens assembly installed in front of the SWIR camera.

4. Fabry-Perot Filter Array

A F-P filter consists of two highly reflective mirrors separated by a spacing or cavity. For fixed wavelength operation, the cavity thickness is equal to one half of the wavelength of light that it transmits. The operation of the F-P filter is based on interference of light. F-P filter arrays have been developed for various applications (*9–12*). In many applications, instead of using two traditional mirrors with high reflectivity coatings, two multilayer dielectric stack mirrors made with alternating high and low refractive index transparent materials are used. The performances of the F-P filter array used in multispectral imagers should be characterized for the following four major parameters: bandwidth, FWHM, peak transmittance, and the transmittance round the peak. Modeling several choices of materials for the dielectric mirrors used in the F-P filters operating in the 1.5 to 1.8 μm region indicated that the best choice for the dielectric mirrors is

alternating layers of zinc sulfide (ZnS) and SiO_2, however since ITC had no prior experience with ZnS, the next best choice of TiO_2 and SiO_2 was selected for fabrication of dielectric mirrors (*13–15*).

4.1 Modeling of F-P filters

The analysis results carried out using a commercial thin-film modeling software program TFCalc by Software Spectra Inc. (*16*) showed that by choosing a larger number of layers for each mirror, the FWHM of the filter can be narrowed. Many simulations were carried out to understand the effect of change in refractive index of the material until the desired results were obtained. The filter design was optimized by using measured values of refractive indices. In figure 7, values of refractive indices for TiO_2 and SiO_2 obtained from the TFCalc software and also from laboratory measurement are shown as a function of wavelength. Thin layers of TiO_2 and SiO_2 on glass substrate were grown using a Leybold thin-film deposition machine and the refractive indices were measured by a Woollam ellipsometer. These measured values were used in the thin-film coating software to obtain the dielectric stack with desired FWHM. Figure 8 shows the change in FWHM of the filter by using different number of layers in the design of the dielectric mirror. An 11-layer dielectric stack was selected to fabricate each mirror structure, as shown in figure 9. The thickness of the SiO_2 and TiO_2 layers in the mirror was equal to one quarter wavelength at 1650 nm corresponding to the center of the spectral region, while the values of the cavity thickness were approximately equal to half of the center wavelength corresponding to each of the 16 filters.

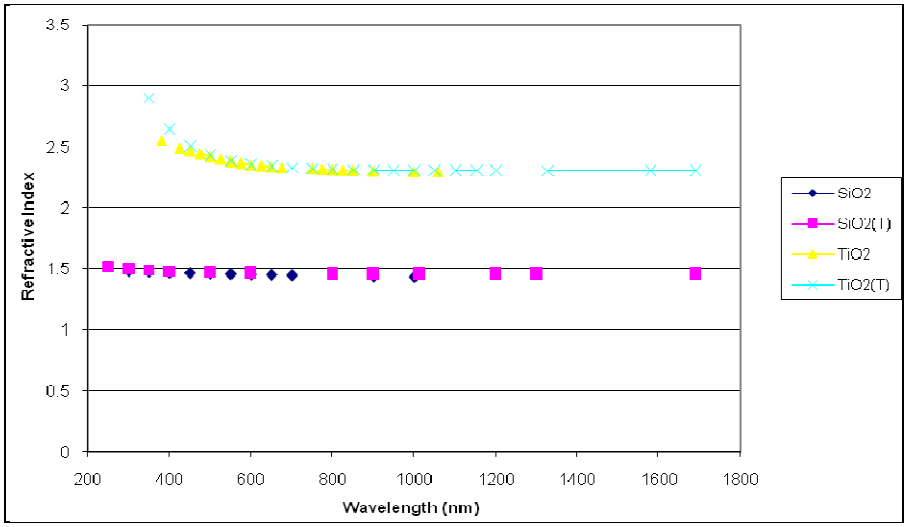

Figure 7. Values of refractive indices of SiO2 and TiO2 shown are from TFCalc software and SiO2(T) and TiO2(T) are from laboratory measurement of thin films of SiO_2 and TiO_2.

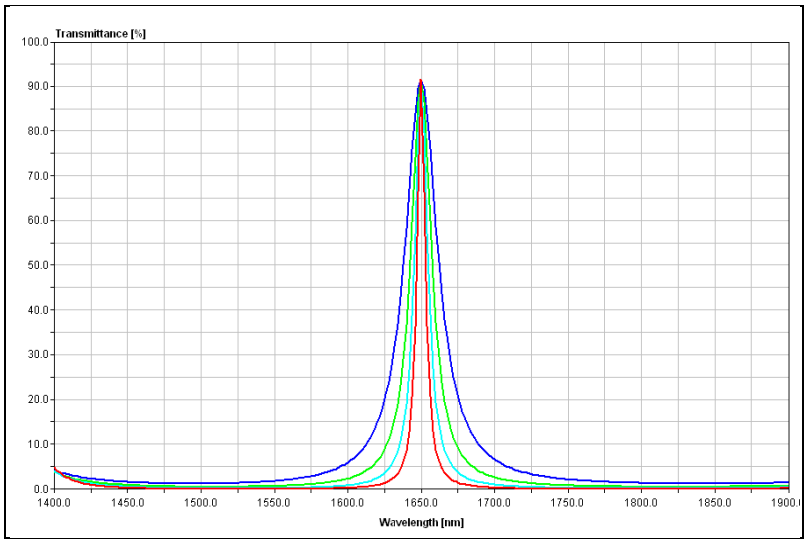

Figure 8. Results of modeling showing FWHM for dielectric mirror operating at 1650 nm with 8 layers (——), 9 layers (——), 10 layers (——), and 11 layers (——) using TFCalc software.

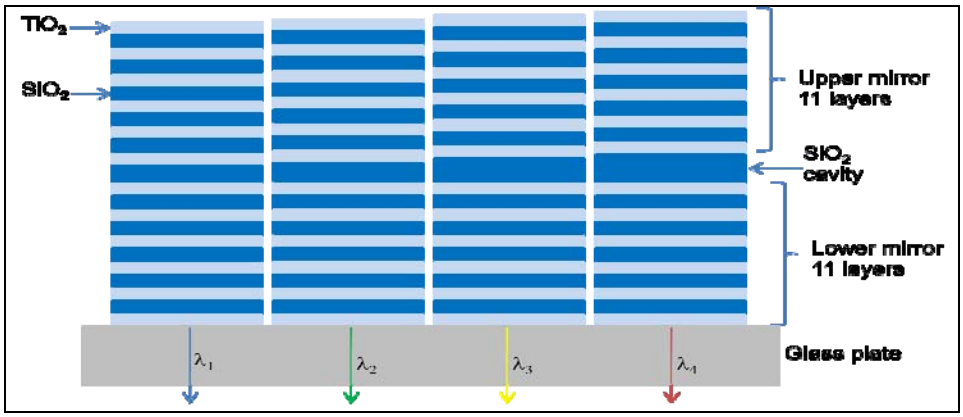

Figure 9. Schematic drawing of the side view of F-P filter array showing four filters operating at λ_1, λ_2, λ_3, and λ_4 wavelengths. Each F-P filter has the same 11 alternating TiO_2 (n = 2.3) and SiO_2 (n = 1.46) layer upper and lower mirrors. The thickness of SiO_2 cavity is different for each wavelength roughly equal to half of the center wavelength of the filter.

Based on the TFCalc simulations of the 11-layer dielectric mirror, it was shown that the each mirror has a reflectance, *R*, of around 98% from 1500 to 1800 nm and the finesse, *F*, of the F-P filter defined by the following well known expression:

$$F = \frac{\pi\sqrt{R}}{(1-R)}, \tag{5}$$

which is high equal to 155.5. The calculated transmission for each F-P filter from 1500 to 1800 nm is around 90% as shown in figure 10. In reality, actual process of fabrication and measurement uncertainties may yield a lower value.

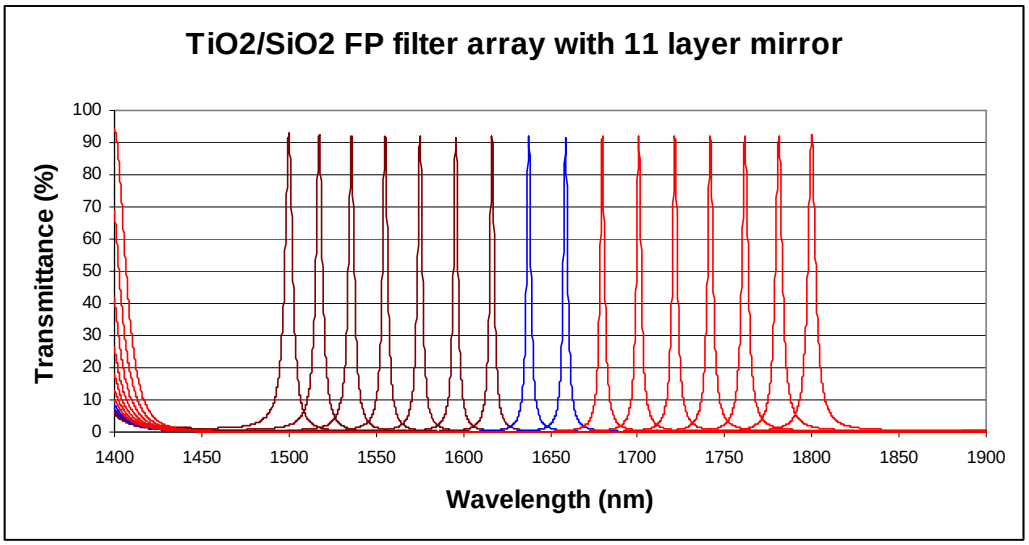

Figure 10. Calculated transmittance of F-P etalon with 11-layer TiO_2/SiO_2 mirrors using TFCalc.

4.2 MEMS F-P Filter Array Fabrication Process

A large number of 4×4 F-P filter arrays were fabricated by using only four masks on a common glass plate. The filter array was fabricated using a Leybold e-beam evaporator system. The TiO_2/SiO_2 layer thicknesses for both the mirror structures for each of the 16 filters in the array were the same, although the cavity thickness was different for each filter in the array. One way to do this is to use 16 separate cavity layer depositions. This requires a total of 18 process steps, which is too many. Thus, the main challenge was to minimize the number of steps involved in depositing 16 different thicknesses of SiO_2 cavity layers for the 16 filters. The approach used here uses far fewer layer deposition steps to achieve this. This was achieved by using a set of four shadow masks, as shown in figure 11, which enabled us to use only six process steps. The first process step used during the film deposition was to deposit the 11-layer TiO_2/SiO_2 bottom mirror, as shown in figure 9, and a base SiO_2 layer was deposited on all the filters controlled by the thickness controller. The middle four steps were used to adjust the cavity thicknesses of the 16 filters, which were controlled by the quartz thickness controller. During these four steps first the shadow masks (a) was used to deposit layer of SiO_2 on filters 2, 4, 6, 8, 10, 12, 14, and 16, then second mask (b) was used to deposit SiO_2 layer on filters 3, 4, 7, 8, 11, 12, 15, and 16, after that the mask (c) was used to deposit SiO_2 layer on filters 5–8, 13–16 and at the end the mask (d) was used to deposit SiO_2 layer on filters 9–16. The last step was to deposit the second mirror structure, which was also controlled by the optical thickness controller. The full size of the filter array is 12.8×9.6 mm with individual filter size of 3.2×2.4 mm.

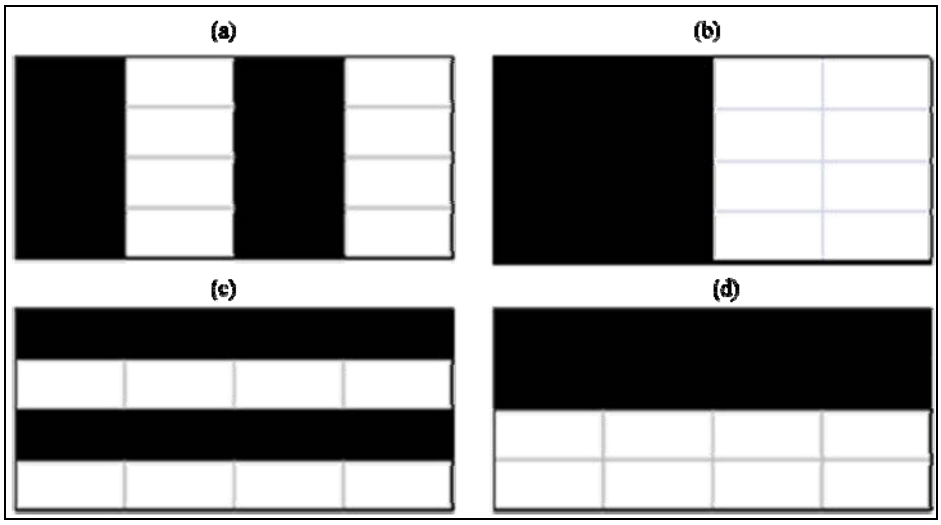

Figure 11. Shown are the four shadow masking steps used to grow the 16 different cavity layers for 16 F-P filters in the array. The mask (a) on the top left is used to grow SiO_2 layer on filters in column 2 and 4, then mask (b) on top right is used to grow SiO_2 layer on filters in columns 3 and 4, next mask (c) on bottom left is to used to grow SiO_2 layer on filters in rows 2 and 4 and the last mask (d) on bottom right is used to grow SiO_2 layer on filters in rows 3 and 4.

The actual shadow masks used to grow the 16 different thicknesses of SiO_2 cavity are shown in figure 12. The numbering system for the filter array on a die is illustrated in figure 13. Scanning electron microscope (SEM) photos of fabricated filter as well as detailed layer structure on a 0.75-mm-thick fused quartz plate is shown in figure 14.

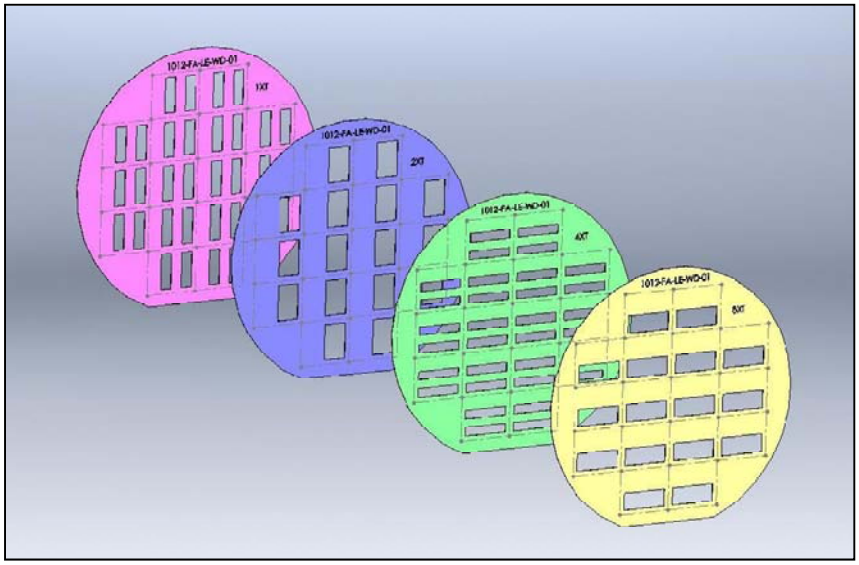

Figure 12. Four shadow masks used to grow the cavities of 16 F-P filters.

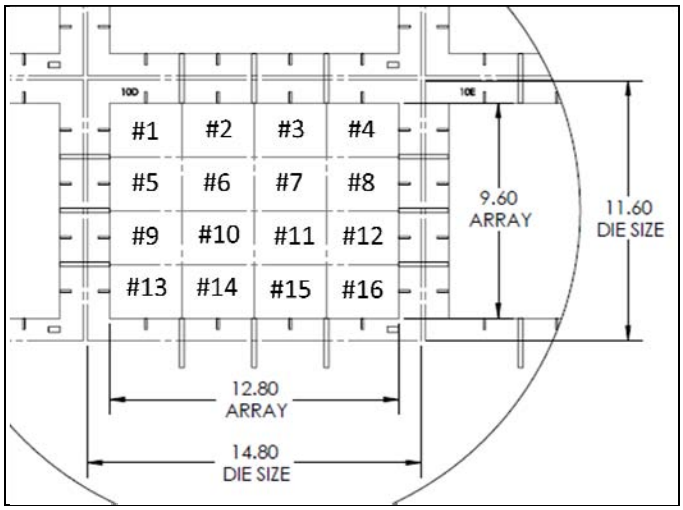

Figure 13. Filter array with numbered filters on a die.

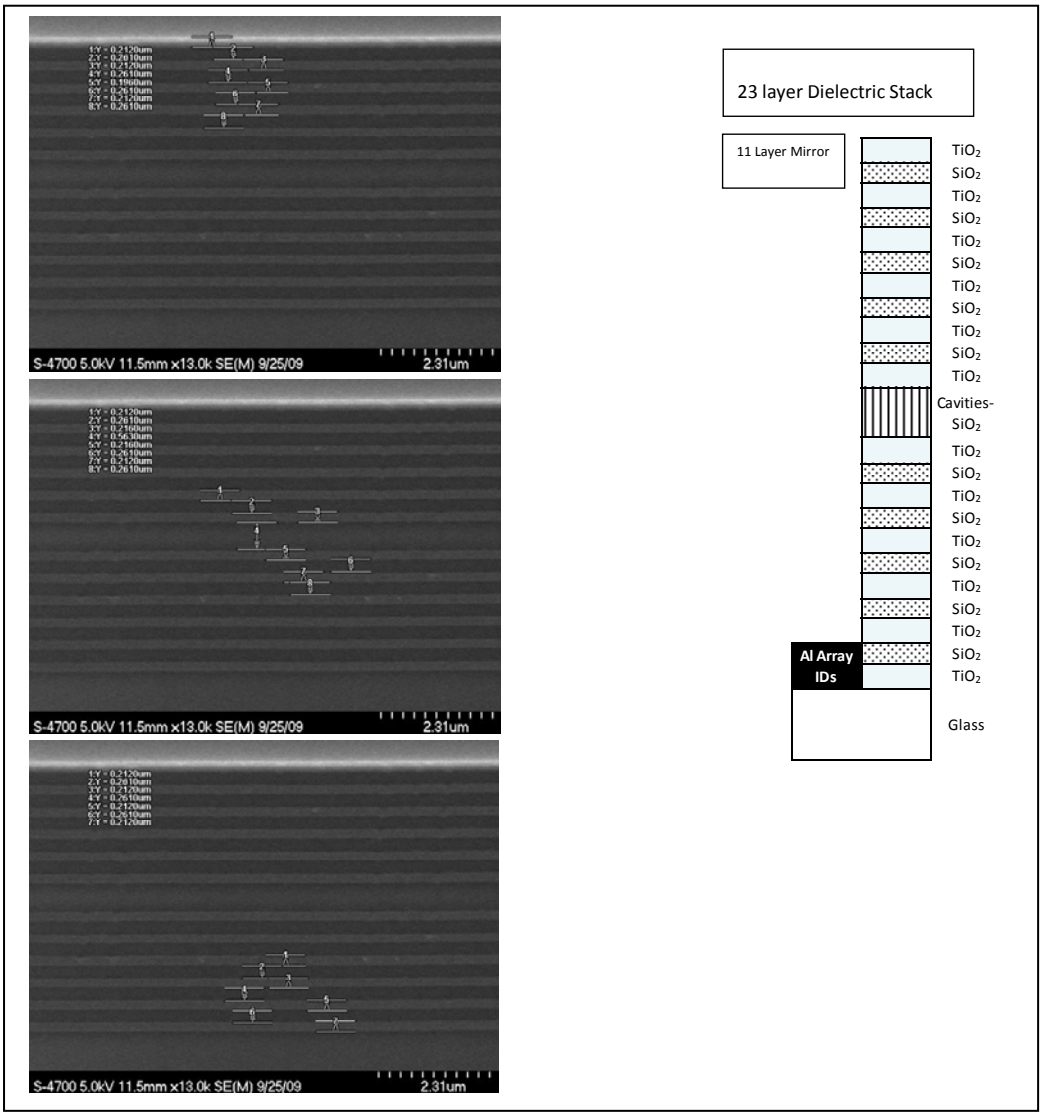

Figure 14. SEM photos of fabricated filter as well as detailed layer structure.

4.3 Experimental Characterization of F-P Filter Array

A fully computer controlled optical setup was used to characterize the spectral properties of the fabricated F-P filter array. It consists of a tunable light source from 320 to 2200 nm with a wavelength accuracy of ±0.6 nm, a fiber bundle, and a power meter with two different detectors. The tunable light source system was a model AST-XE-175-BFEX from Spectral Products with a 175-W xenon light source and a 1/8-meter monochromator. The nominal maximum spectral resolution of the output light is about 1 nm. A Newport dual channel power meter model 2832 – C with both silicon (Si) (model 818-ST) and germanium (Ge) (model 818-IR) detectors was used. The size of the Si detector is 10×10 mm^2 and the diameter of the Ge detector is 3 mm. Since the filter array operates in the 1.5- to 1.8-μm region, the Ge detector was used. The operation of the optical setup, including data collection with a graphical output, was computerized. A computer was used to communicate with the monochromator and the power meter to perform the spectral scan. This setup was used to detect the optical interference peaks, to calibrate the bandwidth resolution and measure the light intensity distribution across the F-P filters.

Figure 15 is a schematic of the test system. The light output from monochromator is coupled into a fiber bundle with an entrance slit size of 0.2×4.2 mm and an output circle with a diameter of 1 mm. The detector is mounted on a linear stage in order to move the detector "in" and "out." When the detector is at "in" position, the optical spectrum can be scanned. The active area of detectors is large enough to collect the entire light beam. When the detector is at "out" position, image of the sample (labeled TF) can be observed on the monitor through the lens and charge-coupled device (CCD) camera for carrying out optical alignment.

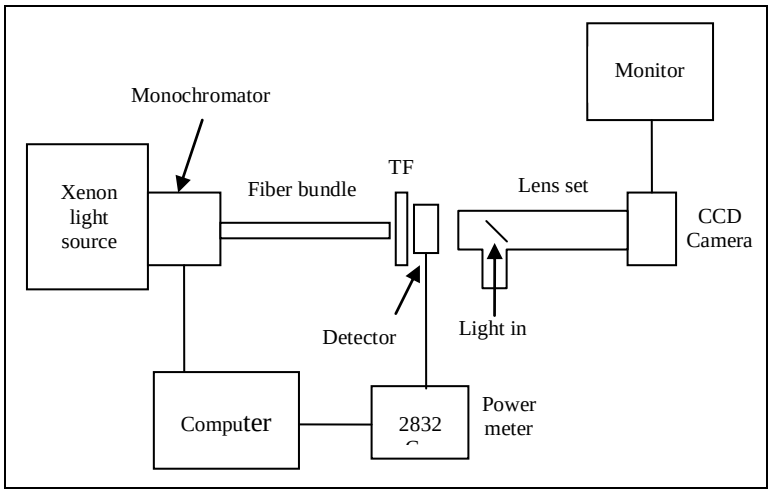

Figure 15. Optical setup used to characterize filter array and imager.

The filter test system was calibrated using commercial inference filters of known bandpass values with center wavelengths: 1460, 1555, 1670, 1723, 1810, and 1900 nm, as shown in figure 16. The spectral transmission of each of the fabricated F-P filter in the filter array was measured with the above optical setup, as shown in figure 17.

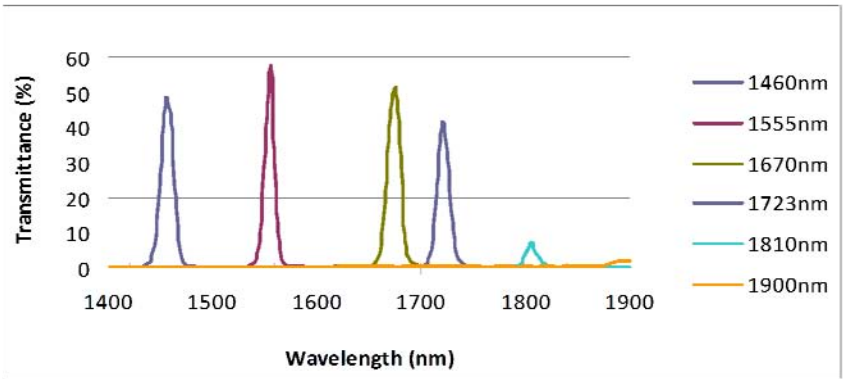

Figure 16. Measured transmission spectra of interference filters used to calibrate the optical test setup.

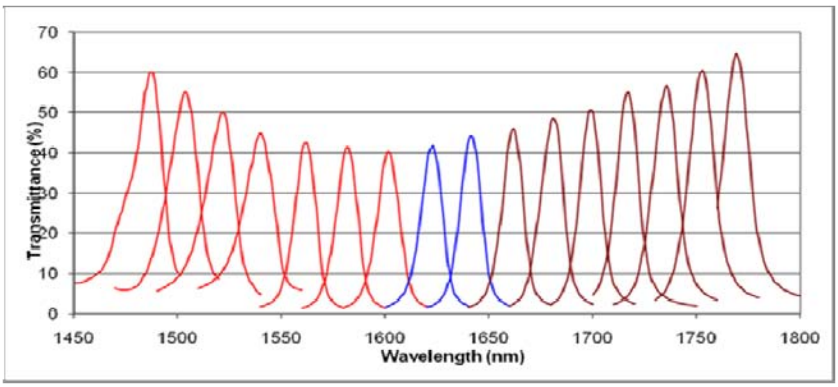

Figure 17. Measured spectral transmission of each of the 16 spectral channels in the filter array.

5. Snapshot Multispectral Imager

The camera lens of one InGaAs camera model SU3201.7RT with a 320×240 FPA was removed. The fabricated F-P filter array was installed in front of the FPA and then the microlens assembly was installed in front of the filter array, as shown in figure 1, to obtain the snapshot imager with 16 spectral channels. A long-wave cutoff filter was also installed to block the shorter wavelength light. A photograph of the snapshot multispectral imager is shown in figure 18. The camera was then used to image a number of indoor and outdoor scenes.

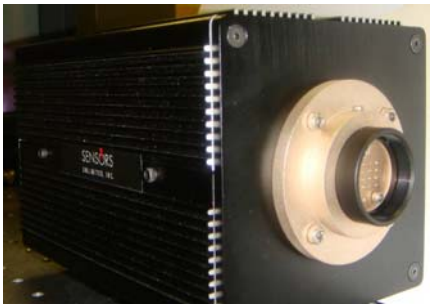

Figure 18. Snapshot multispectral imager with 16 spectral channels as shown in figure 17.

6. Results and Analysis

Table 1 lists the specifications of the filter array. Both the target specifications and corresponding measurement results are listed for comparison. It is quite clear from this table that the measurement results are quite close to the target specifications. The measured bandpass of each of the 16 filters was quite narrow (12–18 nm), as shown in figure 14 and listed in table 1. The measured transmittance of each of the filter in the array, as shown in figure 17, was far below the predicted value of 90% shown in figure 10 even though it met the target specification. One of the main reasons for this reduced value is the uneven thickness of the thin films grown for the multilayer dielectric mirror and another reason is the lower resolution of the measurement system shown in figure 15 due to the short length (1/8 m) of the monochromator used, which can be accounted for by analyzing the results for calibrated interference filters shown in figure 16. The vendor specified value for 1460 nm filter is 70% while the measured value shown in figure 16 is around 50%. When this is taken into account, the effective transmission should be at least 40% more than the values shown in figure 17. Another reason for getting lower value of transmittance in the measurement is due to not applying antireflection coating on the filter array. These problems will be fully addressed in near future to improve optical transmission of filters.

Table 1. Specifications of F-P filters.

Parameter	Target Specification	Measurement Results
Spectral region (nm)	1500–1800	1487–1769
Width of spectral region(nm)	300	282
Peak to peak separation (nm) for 16 channels	20	16–22
FWHM for each channel (nm)	10–15	12–18 FP1 -18, FP2 - 17, FP3 - 17, FP4 - 18, FP5 - 13, FP6-13, FP7 - 13, FP8 - 13, FP9 - 12, FP10 - 12, FP11 - 13, FP12 - 14, FP13 - 13, FP14 - 14, FP15 - 15, FP16 - 16
Filter peak wavelength for each channel (nm)		FP1-1487, FP2 - 1504, FP3 - 1522, FP4 - 1540, FP5 - 1562, FP6 - 1582, FP7 - 1601, FP8 - 1623, FP9 - 1641, FP10 - 1662, FP11 - 1681, FP12 - 1699, FP13 - 1717, FP14 - 1736, FP15 - 1753, FP16 - 1769
Peak transmittance (%)	>40	50–90 (corrected)

The imager shown in figure 18 was used to image a number of indoor and outdoor scenes. Some examples of images obtained from this imager are shown in figures 19 and 20. It is clear from these images that each spectral channel operated independently without noticeable out-of-band leakage and the dark pixels between the sub images are due to the baffle. The sub images seem to be slightly tilted due to misaligned placement of the filter array on the FPA and is quite easy to fix.

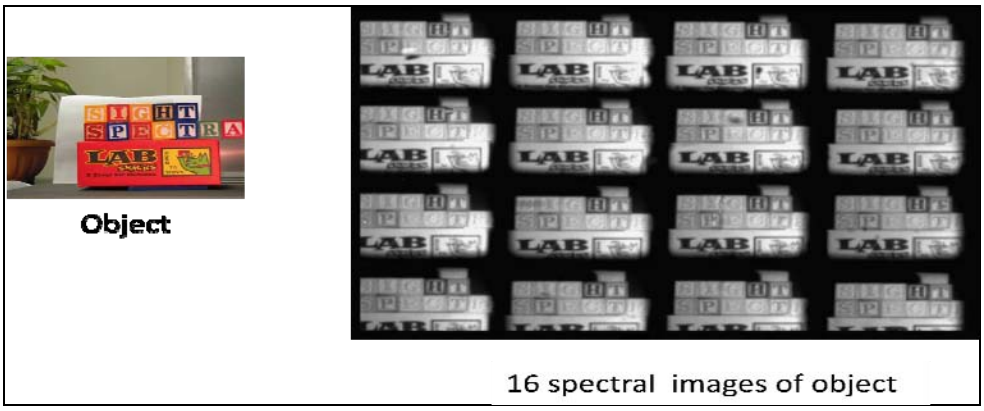

Figure 19. Sixteen spectral images of the object on the left obtained with the snapshot imager.

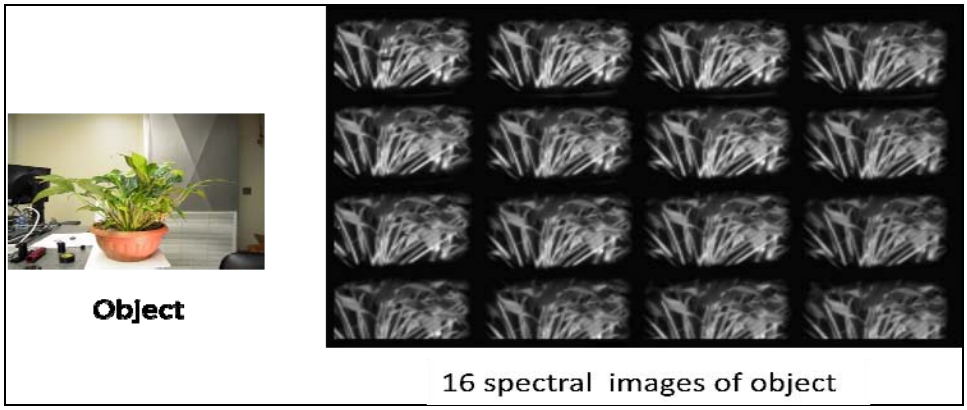

Figure 20. Sixteen spectral images of the plant on the left obtained with the snapshot imager.

A fiber optic bundle was used as a variable wavelength target to demonstrate the spectral performance of the multispectral camera system. Figure 21 shows the image of the fiber bundle holder. The fiber bundle was illuminated from 1400 to 1900 nm in 5-nm increments. Screen captures of the video that show the light cycling from filter #1 position to filter #16 were created and pasted in figures 22–37. Each image has 16 images of the fiber-optic bundle and holder and only the proper wavelength corresponding to the filter passband lights up.

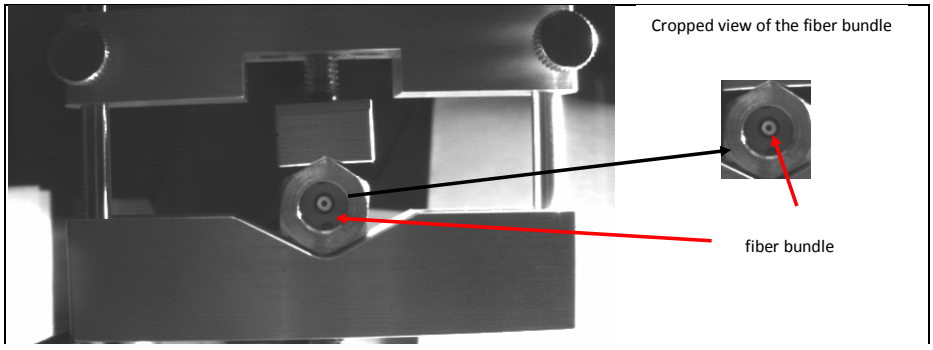

Figure 21. Cropped view of a fiber optic bundle holder.

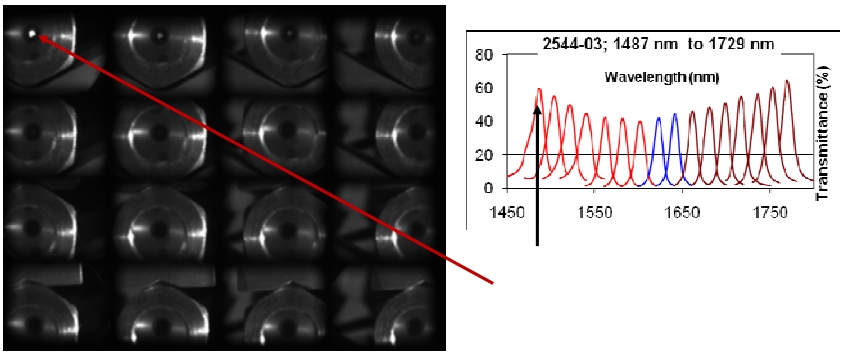

Figure 22. Fiber at filter # 1, 1487 nm.

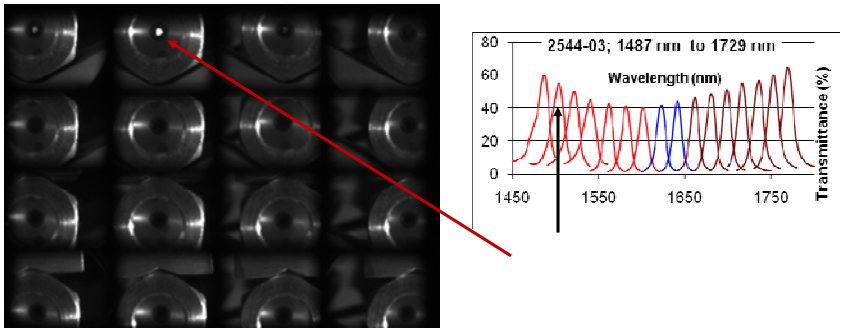

Figure 23. Fiber at filter # 2, 1504 nm.

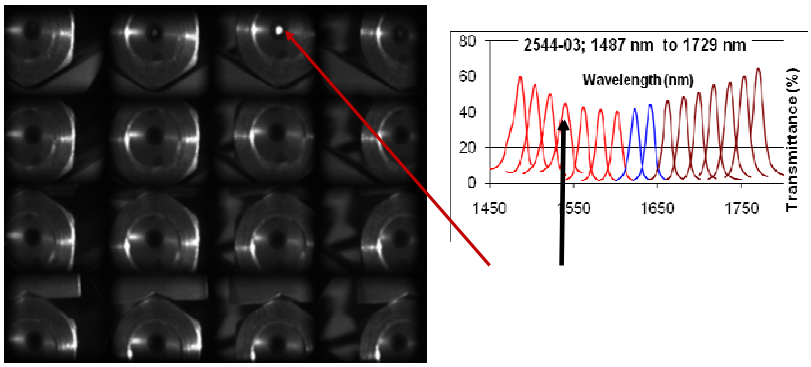

Figure 24. Fiber at filter # 3, 1522 nm.

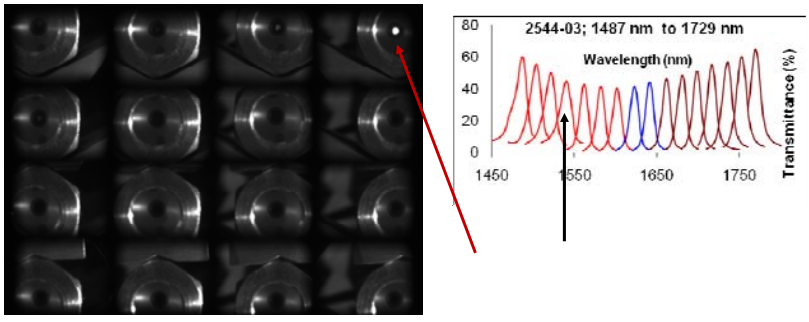

Figure 25. Fiber at filter # 4, 1540 nm.

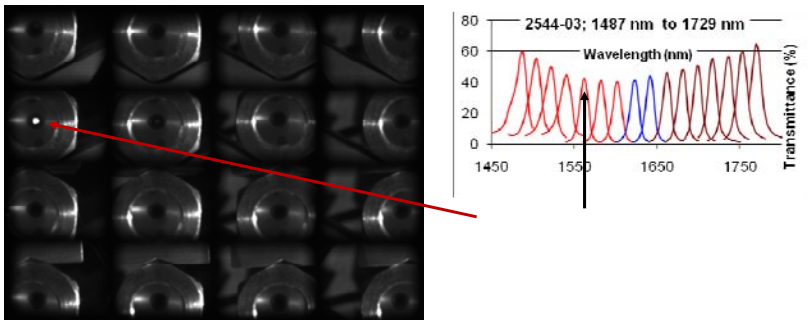

Figure 26. Fiber at filter # 5, 1562 nm.

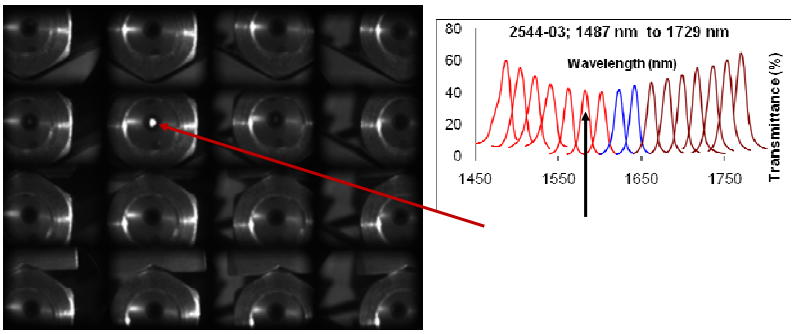

Figure 27. Fiber at filter # 6, 1582 nm.

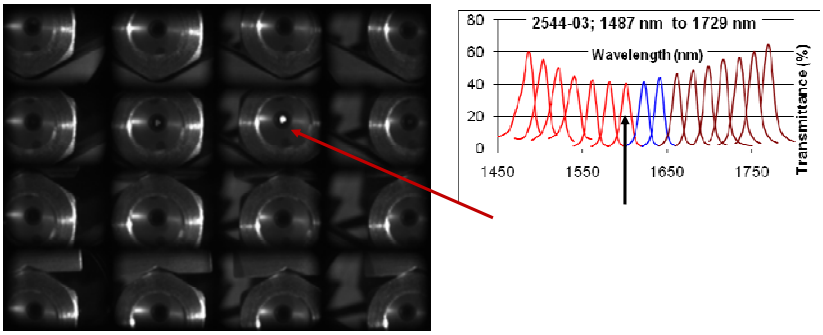

Figure 28. Fiber at filter # 7, 1601 nm.

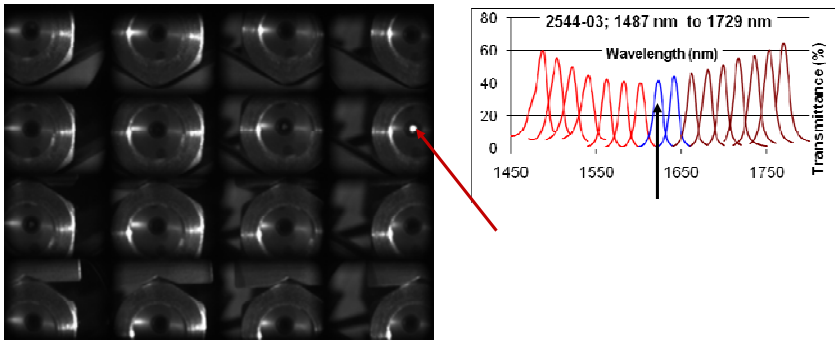

Figure 29. Fiber at filter # 8, 1623 nm.

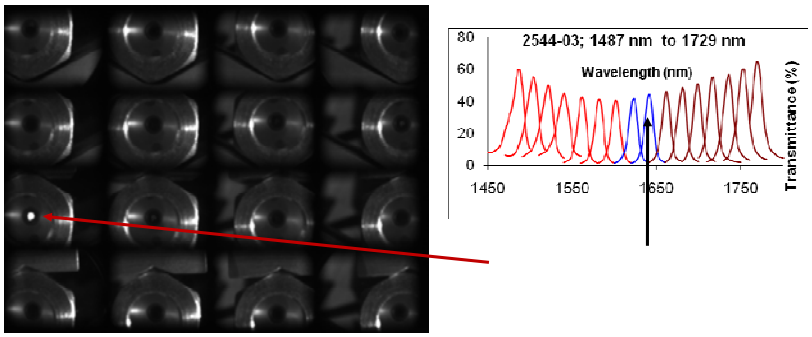

Figure 30. Fiber at filter # 9, 1641 nm.

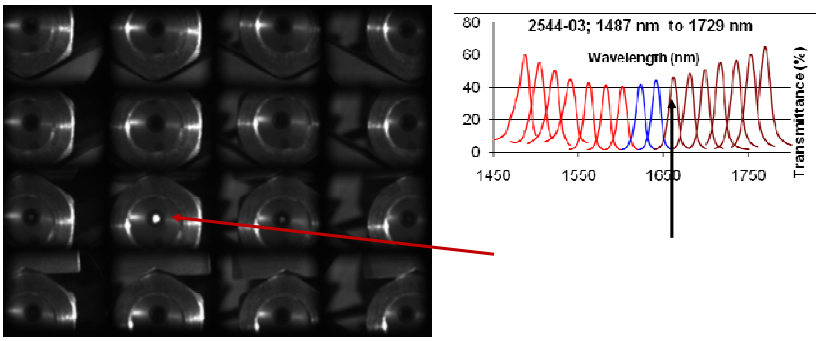

Figure 31. Fiber at filter # 10, 1662 nm.

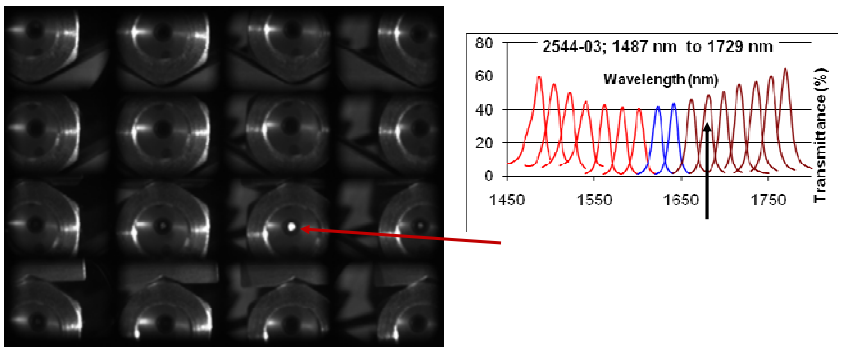

Figure 32. Fiber at filter # 11, 1681 nm.

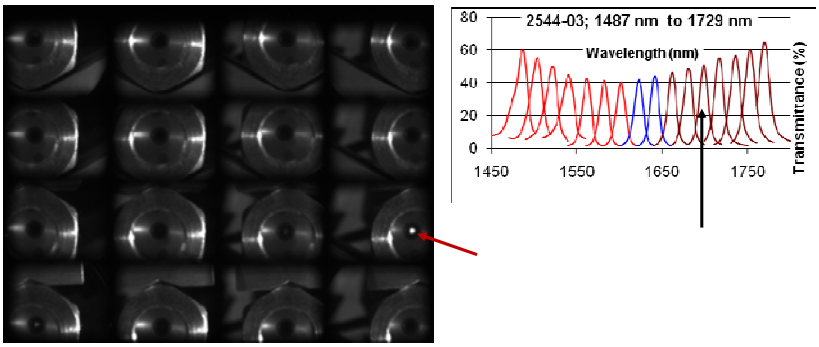

Figure 33. Fiber at filter # 12, 1699 nm.

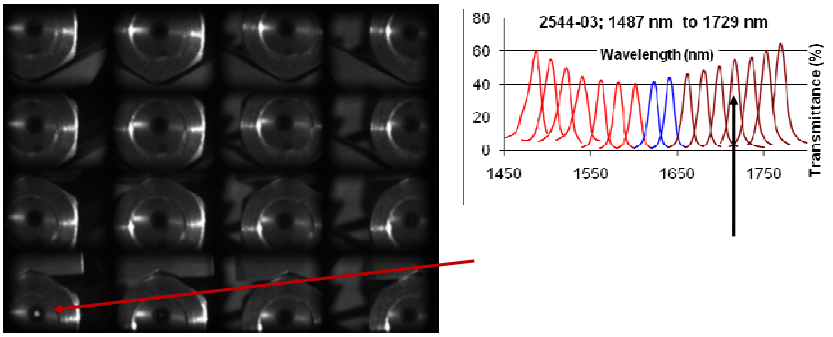

Figure 34. Fiber at filter # 13, 1717 nm.

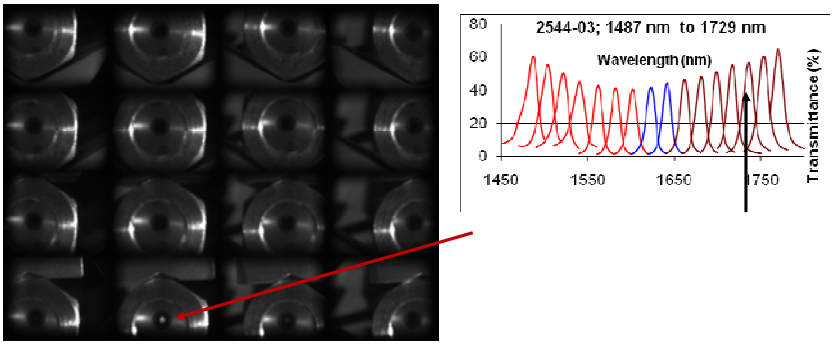

Figure 35. Fiber at filter # 14, 1736 nm.

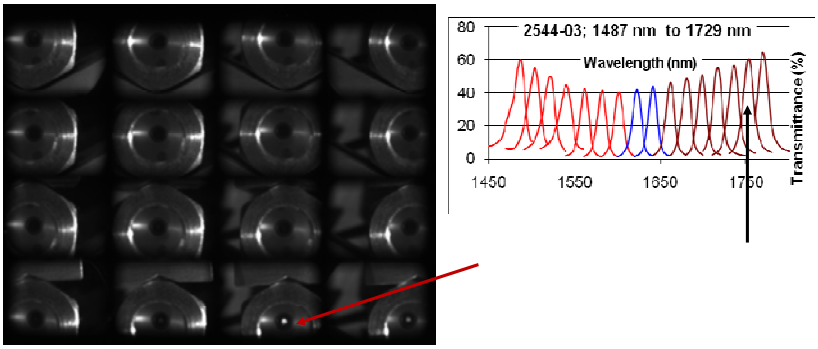

Figure 36. Fiber at filter # 15, 1753 nm.

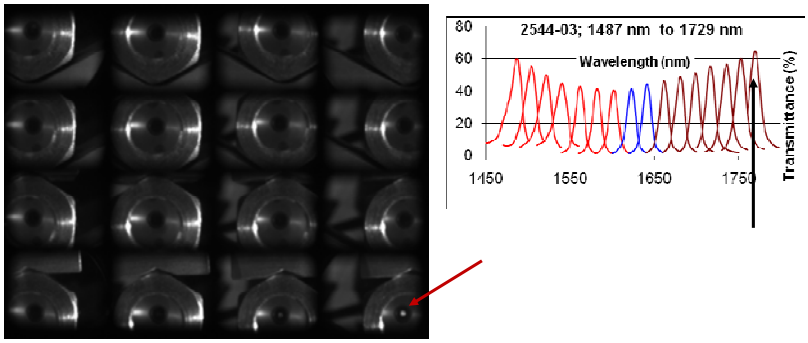

Figure 37. Fiber at filter # 16, 1779 nm.

This experiment clearly validated that the multispectral imager is working over the entire range of wavelength of operation from 1487 to 1779 nm.

7. Summary and Conclusions

A miniature multispectral snapshot imager with 16 spectral channels operating in the SWIR region (1.5–1.8 μm) was developed using a fabricated F-P etalon based filter array, custom designed optical frontend, and a commercial SWIR camera with an InGaAs FPA. The filter array was fabricated using MEMS shadow mask technology using only 4 masks to grow 16 different cavity thicknesses for the filter array. The filter array met the target specifications and in future even greater performance can be obtained by making some minor changes in the fabrication process. A 16-channel optical frontend assembly that replaced the camera lens was fabricated to obtain independent spectral image from each channel. The present frontend optics uses machined commercial lenses with honeycomb baffles and light stops to ensure telecentric light propagation and minimize out of band spillage on each of the 16 spectral channels. In future, monolithic microlens arrays will be used in the optical assembly, which will reduce the cost further and the optics will become more ruggedized. The filter and frontend optics designs are quite flexible and can be modified to meet a variety of operational requirements and mission needs. Many different scenes were imaged and high quality spectral images were obtained. The snapshot imager will be used to carry out chemical analysis in the near future.

The snapshot multispectral imager design described here is extremely versatile and adaptable to meet the requirements of different optical bands, FPAs, camera hardware, and bandpasses. The MEMS-based fabrication process is quite easy to implement and cost effective and can be tailored to design a number of custom snapshot imagers for a variety of applications. Automating the image analysis would greatly enhance the performance of the multispectral imager.

8. References

1. Hinnrichs, M; Morris, G. M. Image multispectral sensing, U.S. patent 5479258, 1995.
2. Volin, C. E.; Garcia, J. P.; Dereniak, E. L.; Descour, M. R.; Hamilton, T.; McMillan, R. Midwave-Infrared Snapshot Imaging Spectrometer. *Appl. Opt.* **2001**, *40*, 4501–4506.
3. Mathews, S. A. Design and Fabrication of a Low-cost, Multispectral Imaging System. *Appl. Opt.* **2008**, *47*, F71–F76.
4. Gao, L.; Kester, R. T.; Tkaczyk, T. S. Compact Image Slicing Spectrometer (ISS) for Hyperspectral Fluorescence Microscopy. *Opt. Express* **2009**, *17*, 12293–12308.
5. Kong, L.; Sprigle, S.; Yi, D.; Wang, C.; Wang, F.; Liub, F.; Wang, J.; Zhao, F. Detecting Early Stage Pressure Ulcer on Dark Skin Using Multi Spectral Imager. *Proc. SPIE*, vol. 7494, 74940Q, 2009.
6. Goodrich/Sensors Inc. Web site. http://www.sensorsinc.com/cameras.html (accessed July 2010).
7. Mir J.; Boysel, M. R. High Speed, Optically-Multiplexed, Hyperspectral Imagers and Methods Thereof, U.S. Patent Application 11/995362, 2008.
8. Smith, W. J. *Modern Optical Engineering*, Chapter *8*; McGraw-Hill Professional, 2000.
9. Jayaraman; et al. WDM Multiplexer – Demultiplexer Using Fabry – Perot Filter Array. U.S. Patent 5835517 (1998).
10. Minas, G.; Ribeiro, J. C.; Martins, J. S.; Wolffenbuttel, R. F.; Correia, J. H. An Array of Fabry – Perot Optical – Channels for Biological Fluids Analysis. *Sensors and Actuators A: Physical* **2004**, *115*, 362–367.
11. Correia, J. H.; Bartek, M.; Wolffenbuttel, R. F. High-selectivity Single-chip Spectrometer for Operation at Visible Wavelengths. *Electron Devices Meeting, 1998 – IEDM '98 : Technical Digest, International*, 1988, 467–470.
12. Guy, D.R.P.; Taylor, L. L.; Bass, S. J.; Apsley, N. High Quality InP/InGaAs Fabry-Perrot Etalons Grown by AP MOCVD. *Semicon. Sci. Technol.* **1987**, *2*, 466–467.
13. Szipocs, R.; Ferencz, K. Chirped Multilayer Coatings for Broadband Dispersion Control in Femtosecond Lasers. *Opt. Letts.* **1994**, *19*, 201–203.
14. Netterfield, R. P.; Schaeffer, R. C.; Sainty, W. G. Coating Fabry-Perot Interferometer Plates with Broadband Multilayer Dielectric Mirrors. *App. Opt.* **1980**, *19*, 3010–3017.

15. Chinnayelka, S.; Bessler, R. S.; McShane, M. J. Modeling and Fabrication of Mirrors used in Microspectrometers for Infrared Analysis of Biofluids. *Proc. 2nd Joint EMBS/BMES Conference*, 2002, 1658–1659.

16. Software Spectra Inc. Web site http://www.sspectra.com/ (accessed March 2010).

List of Symbols, Abbreviations, and Acronyms

ARL	U.S. Army Research Laboratory
F-P	Fabry-Perot
FPA	focal plane array
FWHM	full width at half maximum
IEDs	improvised explosive devices
ITC	Infotonics Technology Center
LWIR	long-wave infrared
MEMS	microelectromechanical system
SEM	scanning electron microscope
SiO_2	silicon dioxide
SWIR	shortwave infrared
UV	ultraviolet

NO. OF COPIES	ORGANIZATION
1 ELEC	ADMNSTR DEFNS TECHL INFO CTR ATTN DTIC OCP 8725 JOHN J KINGMAN RD STE 0944 FT BELVOIR VA 22060-6218
1 CD	OFC OF THE SECY OF DEFNS ATTN ODDRE (R&AT) THE PENTAGON WASHINGTON DC 20301-3080
1	US ARMY RSRCH DEV/ENGRG CMD ARMAMNT RSRCH DEV/ENGRG CTR ARMAMNT ENGRG/TECH CTR ATTN AMSRD AAR AEF T J MATTS BLDG 305 APG MD 21005-5001
1	PM TIMS, PROFILER (MMS-P) AN/TMQ-52 ATTN B GRIFFIES BUILDING 563 FT MONMOUTH NJ 07703
1	US ARMY INFO SYS ENGRG CMND ATTN AMSEL IE TD A RIVERA FT HUACHUCA AZ 85613-5300
1	COMMANDER US ARMY RDECOM ATTN AMSRD AMR W C MCCORKLE 5400 FOWLER RD REDSTONE ARSENAL AL 35898-5000
1	US GOVERNMENT PRINT OFF DEPOSITORY RECEIVING SECTION ATTN MAIL STOP IDAD J TATE 732 NORTH CAPITOL ST NW WASHINGTON DC 20402
1	INFOTONICS TECHNOLOGY CENTER ATTN S TAN 5450 CAMPUS DRIVE CANANDAIGUA NY 14424

NO. OF COPIES	ORGANIZATION
1	SPECTRALSIGHT INC ATTN P ASHE 2 MAE MEADOW ROCHESTER NY 14624
2	US ARMY RSRCH LAB ATTN RDRL CIM G T LANDFRIED ATTN RDRL WML A A MIZIOLEK BLDG 4600 APG MD 21005-5066
21	US ARMY RSRCH LAB ATTN IMNE ALC HRR MAIL & RECORDS MGMT ATTN RDRL CIM L TECHL LIB ATTN RDRL CIM P TECHL PUB ATTN RDRL SE J PELLEGRINO ATTN RDRL SEE G WOOD P GILLESPIE L BLISS ATTN RDRL SEE E N GUPTA K ALIBERTI B STANN P MILOJKOVIC ATTN RDRL SEE I P UPPAL D BEEKMAN P WIJEWARNASURIYA ATTN RDRL SEE R J MAIT ATTN RDRL SES A N SROUR R SARTAIN ATTN RDRL SER L M DUBEY ATTN RDRL SES E R RAO D ROSARIO ATTN RDRL SER U K KAPPRA ADELPHI MD 20783-1197
1	DARPA MTO ATTN N DHAR 3701 NORTH FAIRFAX DR ARLINGTON VA 22203-174
3	RDECOM ECBC JIM JENSEN JANET JENSEN WILLIAM LOEROP BLDG E5554 APG MD 21010-5424

NO. OF COPIES	ORGANIZATION
1	RDECOM-TARDEC BRIAN J COLLINO RDTA-RS/MS 271 6501E 11 MILE ROAD WARREN MI 48397-5000
2	TEDT-AT-WFT FRANK CARLEN LUAN HUYNH ABERDEEN TEST CENTER 400 COLLERAN ROAD APG MD 21005-5059
1	AFRL/MNGG DONALD SNYDER 101 WEST EGLIN BLVD., BLDG 13 EGLIN AFB FL 32542-6810
1	SPECTRALSIGHT, INC. PHILIP R. ASHE 2 MAE MEADOW ROCHESTER NY 14624
3	ITC SONGSHENG TAN NANCY STOFFEL PAUL TOLLEY 5450 CAMPUS DR. CANADAIGUA NY 14424
2	ARMY RESEARCH OFFICE ATTN RDRL ROE L W CLARK ATTN RDRL ROE V R HARMON BUILDING 4300 RM 238 RESEARCH TRIANGLE PARK NC 27703
1	ARMY RESEARCH OFFICE - ALEXANDRIA (ARO-E(A)) ATTN RDRL RO J HARVEY ALEXANDRIA VA 22333-001

TOTAL: 47 (1 ELEC, 1 CD, 45 HCS)